THE ANNALS OF "DUNĂREA DE JOS" UNIVERSITY OF GALAŢI
FASCICLE V, TECHNOLOGIES IN MACHINE BUILDING,
ISSN 1221- 4566, 2017

NATURAL CONVECTION IN THE BOUNDARY LAYER OF A CONSTANT TEMPERATURE AND CONCENTRATION VERTICAL WALL EMBEDDED IN A DARCY DOUBLY STRATIFIED POROUS MEDIUM

Maria Neagu[1]

[1]"Dunărea de Jos" University of Galaţi, Manufacturing Engineering Department, Galaţi, România
Maria.Neagu@ugal.ro

ABSTRACT

This paper presents the succession of heat and/or mass driven natural convection processes along a uniform temperature and concentration vertical wall embedded in a Darcy doubly stratified porous medium. Using the scale analysis of the governing equations, three possible heat transfer regimes are discovered, presented and quantified through the temperature, concentration and velocity boundary layer thickness, magnitude and location. If S_T and S_C are the porous medium thermal and concentration stratification coefficients and if N is the buoyancy ratio, then we can encounter these possibilities: a heat driven convection regime (HDC) along the wall if $S_C > S_T$; a mass driven convection regime (MDC) along the wall if $S_T > S_C > N > 1$; a HDC−MDC succession in all the other cases. The finite difference method is used to solve the governing equations and to verify the results on the heat transfer regimes succession for one particular case.

KEYWORDS: porous medium, natural convection, double diffusion, scale analysis, finite difference method

1. INTRODUCTION

The study of the natural convection process triggered by a vertical impermeable wall embedded in a Darcy porous medium has received a great consideration in the last decades [1-12]. The particular case of a constant temperature [1-6] and concentration [7-12] wall was analyzed while the environment was considered as being thermally [3-6] or doubly [12] linearly stratified.

This paper considers the case of a vertical impermeable wall situated in a doubly stratified Darcy porous medium. The temperature and the concentration of a certain constituent are constant at the wall. Using the scale analysis method, this paper establishes the heat and mass driven natural convection regimes succession along the wall as well as the point of the wall where the reverse flow occurs.

2. MATHEMATICAL MODEL

Figure 1 presents the dimensional (Fig. 1(a)) and the dimensionless (Fig. 1(b)) problem. The x ordinate lies along the wall, while the abscissa of the co-ordinate system is normal to the wall.

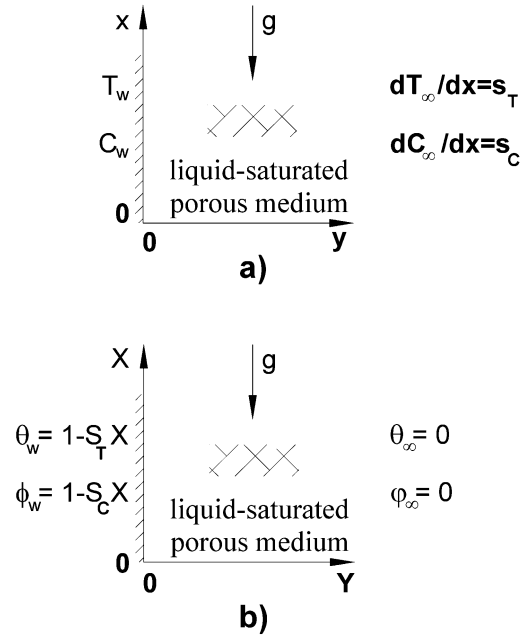

Fig. 1: The vertical wall and the associated coordinate system; (b) the dimensionless domain of the problem. The temperature and the concentration at the wall are constant, T_w and C_w, respectively.

The ambient temperature and concentration vary linearly: $T_{\infty,x} = T_{\infty,0} + s_T x$ and $C_{\infty,x} = C_{\infty,0} + s_C x$, where the stratification coefficients are: $s_T = dT_{\infty,x}/dx$ and $s_C = dC_{\infty,x}/dx$. The fluid density is a variable property; it obeys the Boussinesq approximation:

$$\rho = \rho_0 \left[1 - \beta_T (T - T_{\infty,0}) - \beta_C (C - C_{\infty,0}) \right].$$

The equilibrium governing equations:

$$\frac{\partial v}{\partial x} + \frac{\partial u}{\partial y} = 0 \tag{1}$$

$$\frac{\partial v}{\partial y} - \frac{\partial u}{\partial x} = \frac{K}{\mu}\left[\rho g \beta_t \frac{\partial T}{\partial y} + \rho g \beta_c \frac{\partial C}{\partial y} \right] \tag{2}$$

$$\frac{\partial T}{\partial t} + v\frac{\partial T}{\partial x} + u\frac{\partial T}{\partial y} = \alpha\left(\frac{\partial^2 T}{\partial x^2} + \frac{\partial^2 T}{\partial y^2} \right) \tag{3}$$

$$\frac{\partial C}{\partial t} + v\frac{\partial C}{\partial x} + u\frac{\partial C}{\partial y} = D\left(\frac{\partial^2 C}{\partial x^2} + \frac{\partial^2 C}{\partial y^2} \right) \tag{4}$$

require the following boundary conditions:

$$\begin{aligned} &u = 0,\ T = T_w,\ C = C_w \text{ at } y = 0 \\ &v = 0,\ T = T_{\infty,x},\ C = C_{\infty,x} \text{ as } y \to \infty \\ &v = 0,\ T = T_{\infty,x},\ C = C_{\infty,x} \text{ at } x = 0 \\ &\frac{\partial^2 u}{\partial x^2} = \frac{\partial^2 v}{\partial x^2} = \frac{\partial^2 T}{\partial x^2} = \frac{\partial^2 C}{\partial x^2} = 0 \text{ at } x = h \end{aligned} \tag{5}$$

In Eqs. (1-5), u and v are the horizontal and the vertical velocities, t is time, T is temperature, C is the concentration of a constituent, ρ is density, g is the gravitational acceleration, β_t and β_c are temperature and concentration expansion coefficients, α is thermal diffusivity, while D is mass diffusivity, h is the height of the computational domain. The dimensionless variables:

$$X = \frac{x}{L},\ Y = \frac{y}{L},\ \theta = \frac{T - T_{\infty,x}}{T_w - T_{\infty,0}},\ \varphi = \frac{C - C_{\infty,x}}{C_w - C_{\infty,0}},$$
$$\tau = \frac{t\alpha}{L^2},\ U = \frac{u}{\alpha}L,\ V = \frac{v}{\alpha}L \tag{6}$$

lead us to the dimensionless governing equations:

$$\frac{\partial V}{\partial X} + \frac{\partial U}{\partial Y} = 0 \tag{7}$$

$$\frac{\partial V}{\partial Y} - \frac{\partial U}{\partial X} = Ra\left(\frac{\partial \theta}{\partial Y} + N\frac{\partial \varphi}{\partial Y} \right) \tag{8}$$

$$\frac{\partial \theta}{\partial \tau} + V\frac{\partial \theta}{\partial X} + VS_T + U\frac{\partial \theta}{\partial Y} = \frac{\partial^2 \theta}{\partial X^2} + \frac{\partial^2 \theta}{\partial Y^2} \tag{9}$$

$$\frac{\partial \varphi}{\partial \tau} + V\frac{\partial \varphi}{\partial X} + VS_C + U\frac{\partial \varphi}{\partial Y} = \frac{1}{Le}\left(\frac{\partial^2 \varphi}{\partial X^2} + \frac{\partial^2 \varphi}{\partial Y^2} \right), \tag{10}$$

where $Ra = \left[Kg\beta_t (T_w - T_{\infty,0}) L^3 / \alpha\nu \right]$ is the Rayleigh number, $Le = (\alpha / D)$ is the Lewis number and $N = \left[\beta_c (C_w - C_{\infty,0}) / \beta_t (T_w - T_{\infty,0}) \right]$ is the buoyancy ratio, $S_T = \left[s_T L / (T_w - T_{\infty,0}) \right]$ and $S_C = \left[s_C L / (C_w - C_{\infty,0}) \right]$ are the thermal and the concentration dimensionless stratification parameters.

The dimensionless boundary conditions are:

$$\begin{aligned} &U = 0,\ \theta = 1 - S_T \cdot X,\ \varphi = 1 - S_C \cdot X \text{ at } Y = 0 \\ &V = 0,\ \theta = \varphi = 0 \text{ as } Y \to \infty \\ &V = 0,\ \theta = \varphi = 0 \text{ at } X = 0 \\ &\frac{\partial^2 U}{\partial X^2} = \frac{\partial^2 V}{\partial X^2} = \frac{\partial^2 \theta}{\partial X^2} = \frac{\partial^2 \varphi}{\partial X^2} = 0 \text{ at } X = H \end{aligned} \tag{11}$$

The dimensionless conservation equations, Eqs. (7)-(10), will be analyzed using the scale analysis method [13] in section 3, while section 4 verifies this analysis using the finite differences method [14, 15] applied to the mathematical model.

3. SCALE ANALYSIS

3.1. The natural convection regime types

The scale analysis [13] assumption for both temperature and concentration boundary layers, $\delta_T << X$ and $\delta_C << X$, allows us to neglect the $\partial U / \partial X$ term in Eq. (8):

$$\frac{\partial V}{\partial Y} \sim Ra \cdot \left(\frac{\partial \theta}{\partial Y} \right) + Ra \cdot N \cdot \left(\frac{\partial \varphi}{\partial Y} \right) \tag{12}$$

We integrate Eq. (12) from $Y = 0$ to infinity. The vertical velocity order of magnitude becomes:

$$V \sim Ra \cdot (\Delta\theta) + Ra \cdot N \cdot (\Delta\varphi), \tag{13}$$

where $\Delta\theta$ and $\Delta\varphi$ are the variation of the temperature and the concentration values across the boundary layers thickness. The first term on the right hand side of this Eq. (13), V_T, the vertical velocity due to the volumetric thermal expansion, can be written as:

$$V_T \sim Ra \cdot (\Delta\theta) \cong Ra \cdot (1 - S_T X), \tag{14}$$

while the second term on the right hand side of Eq. (13), V_C, the vertical velocity due to the volumetric concentration expansion, becomes:

$$V_C \sim Ra \cdot N \cdot (\Delta\varphi) \sim Ra \cdot N \cdot (1 - S_C X) \tag{15}$$

As a consequence, the vertical velocity scale is:

$$V \sim Ra \cdot (1 - S_T X) + Ra \cdot N \cdot (1 - S_c X) \qquad (16)$$

The relative magnitude of V_T and V_C, in Eq. (16), defines the natural convection type: HDC (heat driven convection) if $V_T > V_C$ or MDC (mass driven convection) if $V_C > V_T$.

Throughout the scale analysis of this system, the vertical velocity receives the form:

$$V \sim Ra \cdot (1 - S_T X)\delta_1 + Ra \cdot N \cdot (1 - S_c X)\delta_2, \qquad (17)$$

where δ_1 is 1.0 in the HDC regime and 0.0 otherwise. The reverse is true for δ_2.

The analysis of Eq. (16) shows the following possibilities:

– if $X < min(1/S_T, 1/S_C)$, both terms of the right hand side of Eq. (16) are positive. We have a mass driven convection regime (MDC) if $V_C > V_T$ or

$$X > X_1 = \frac{1 - N}{S_T - NS_C} \qquad (18)$$

– the velocity becomes negative indicating a reverse flow if

$$X > X_2 = \frac{1 + N}{S_T + NS_C} = UL \qquad (19)$$

X_2 is the location on the wall where the scale analysis ceases to be valid (UL=" upper limit ").

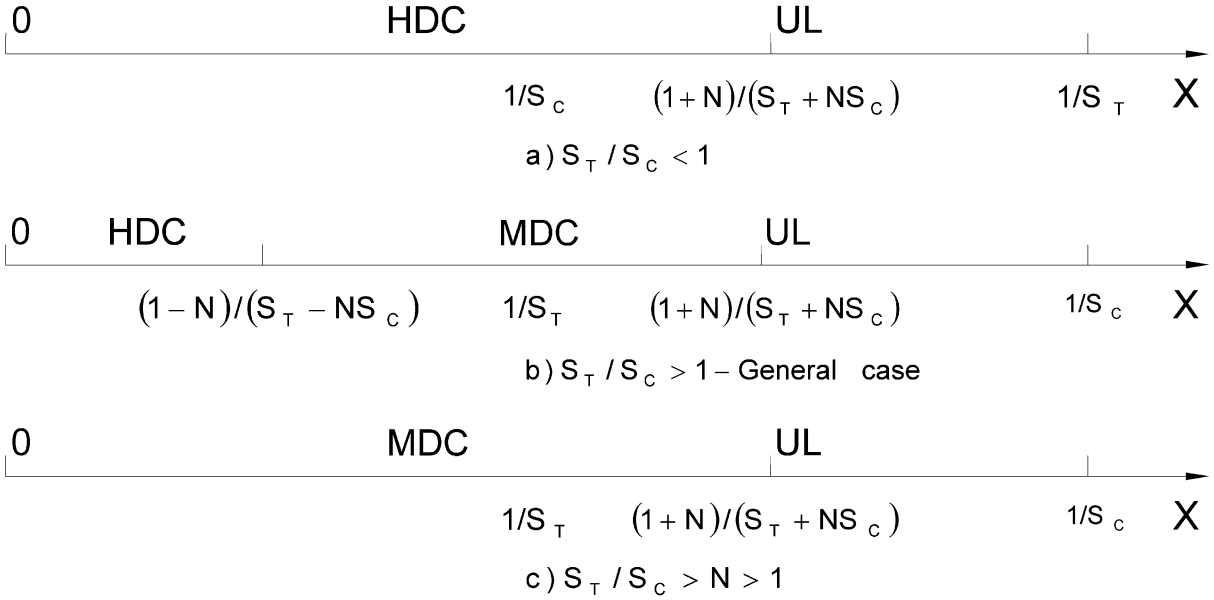

Fig. 2: The heat and the mass driven natural convection regimes sequence. a) $S_T / S_C < 1$; b) $S_T / S_C > 1 > N$ and $1 > S_T / S_C < N$; c) $S_T / S_C > N > 1$.

The two cases: $S_T < S_C$ and $S_T > S_C$ will be analyzed separately:

a) if $S_T < S_C$ (see Fig. 2a): $X_1 > X_2$ and the entire $[0, UL]$ domain is a HDC region;

b) if $S_T \geq S_C$, two situations are encountered:

b$_1$) $S_T / S_C > 1 > N$ and $1 < S_T / S_C < N$ (Fig. 2b): the $[0, X_1]$ region is a HDC region, while the $[X_1, UL]$ region is a MDC region at the equilibrium state;

b$_2$) $S_T / S_C > N > 1$ (Fig. 2c): $X_1 < 0$ and the $[0, UL]$ domain is a MDC region.

Having in view that the maximum vertical velocity is encountered at the wall, two conclusions can be drawn from the scale analysis presented above:

1. if $S_T > S_C$, around the $X = 1/S_T$ abscissa, negative values of the dimensionless temperature, θ, should be registered no matter the values of all the other parameters; the wall temperature $\theta = 0$ at this particular abscissa;
2. if $S_C > S_T$, around the $X = 1/S_C$ abscissa, negative values of the dimensionless concentration, φ, should be registered no matter the values of all the other parameters; the wall dimensionless concentration is ? $\varphi = 0$ at this particular point.

3.2. The scale analysis of the boundary layer region

3.2.1. Scale analysis of the transient state

In the first moments, the equilibrium between inertia and diffusion in the y direction governs the

Eqs. (9) and (10). The scale analysis reveals the order of magnitude of the temperature and concentration boundary layer thicknesses:

$$\delta_T \sim \tau^{1/2};\ \delta_C \sim \tau^{1/2} / Le^{1/2} \tag{20}$$

3.2.2. Scale analysis of the equilibrium concentration boundary layer

In the concentration field, the equilibrium is attained when the vertical convection term has the same order of magnitude as the horizontal diffusion term. Depending on the dominant vertical convection term, we encounter two situations:

1. the $V \cdot \partial\varphi / \partial X$ term is dominant in Eq. (10). The equilibrium state imposes: $V\Delta\varphi / X \sim \Delta\varphi / Le / \delta_C^2$, an equality that defines the equilibrium time and concentration boundary layer thickness:

$$\tau_{ech,C} \sim X / Ra / \left[(1-S_T X)\delta_1 + N(1-S_C X)\delta_2\right] \tag{2}$$

$$\delta_{ech,C} \sim \sqrt{X / \left\{RaLe / \left[(1-S_T X)\delta_1 + N(1-S_C X)\delta_2\right]\right\}} \tag{2}$$

2. the $V \cdot S_C$ term is dominant in Eq. (10). The equilibrium state is realized when: $VS_C \sim \partial^2\varphi / Le / \partial Y^2$. We obtain the equilibrium time and the concentration boundary layer thickness:

$$\tau_{ech,Sc} \sim (1-S_C X) / Ra / S_C / \left[(1-S_T X)\delta_1 + N(1-S_C X)\delta_2\right] \tag{23}$$

$$\delta_{ech,Sc} \sim \left\{\frac{(1-S_C X) / Ra / Le / S_C}{\left[(1-S_T X)\delta_1 + N(1-S_C X)\delta_2\right]}\right\}^{1/2} \tag{24}$$

3.2.3. Scale analysis of the equilibrium temperature boundary layer

Proceeding similarly, the equilibrium time and boundary layer thickness of the temperature field are established:

1. when the $V \cdot \partial\theta / \partial X$ term is dominant in Eq. (9):

$$\tau_{ech,T} \sim X / Ra / \left[(1-S_T X)\delta_1 + N(1-S_C X)\delta_2\right] \tag{25}$$

$$\delta_{ech,T} \sim \sqrt{X / \left\{Ra / \left[(1-S_T X)\delta_1 + N(1-S_C X)\delta_2\right]\right\}} \tag{26}$$

2. if the $V \cdot S_T$ term is dominant in Eq. (9):

$$\tau_{ech,St} \sim (1-S_T X) / Ra / S_T / \left[(1-S_T X)\delta_1 + N(1-S_C X)\delta_2\right] \tag{27}$$

$$\delta_{ech,St} \sim \left\{\frac{(1-S_T X) / Ra / S_T}{\left[(1-S_T X)\delta_1 + N(1-S_C X)\delta_2\right]}\right\}^{1/2} \tag{28}$$

3.2.4. The T—S_T and C—S_C transition

Figure 3 shows the general shape of the $(\partial\theta / \partial X) / S_T$ variation. If we analyze the $[0, \delta_1]$ region, where the VS_T term is dominant in Eq. (9), at equilibrium, the equality of the order of magnitude of the vertical convection and the horizontal diffusion imposes $VS_T \sim \partial^2\theta / \partial Y^2$ or $VS_T \sim \Delta\theta_1 / \delta_1^2$. But at the point "1", $\partial\theta / \partial X = S_T$ or $\Delta\theta_1 / X = S_T$.

Consequently,

$$V \cdot S_T \sim S_T X / \delta_1^2. \tag{29}$$

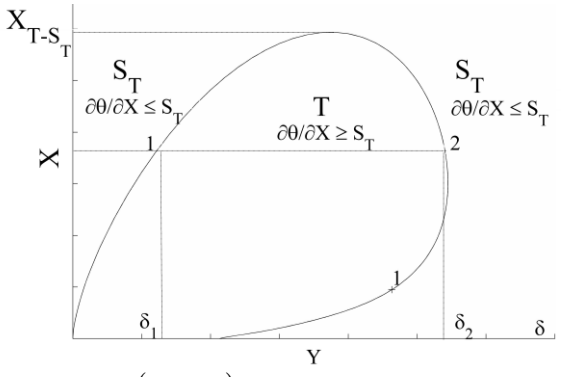

Fig. 3: The $(\partial\theta / \partial X) / S_T$ variation and the T—S_T transition for a Dirichlet boundary condition.

Similarly, in the region situated beyond the point "2" , at the right side of the boundary layer, the equilibrium state requires: $V\left[(\delta - \delta_2)/\delta\right] \cdot S_T \sim \Delta\theta_2 / (\delta - \delta_2)^2$. In the point "2", $\partial\theta / \partial x = S_T$ or $\Delta\theta_2 / X = S_T$. We obtain:

$$VS_T (\delta - \delta_2)^3 / \delta \sim S_T X \tag{30}$$

As we are interested in finding the abscissa, $X_{T—ST}$, where the T—S_T transition occurs, we are imposing:

$$V \cdot S_T \sim \Delta\theta / \delta^2 \tag{31}$$

$$\delta_1 = \delta_2 \tag{32}$$

From Eq. (30) and Eq. (31), we obtain:

$$X_{T-St} = 0.156 / S_T = m / S_T, \tag{33}$$

where m is a constant number: $m = 0.156$.

Similarly, the C—S_C transition is marked by the abscissa

$$X_{C-Sc} = 0.156 / S_C = m / S_C \tag{34}$$

3.2.5. The validity of the scale analysis

The analysis of Fig. 2 and of the points m / S_T and m / S_C, where the T—S_T and C—S_C transitions take place, shows that these abscissas are placed in the HDC regions for the cases presented by

Fig. 2(a) and Fig. 2(b) and only in the case of Fig. 2(c) these transitions take place in the MDC regime.

- If $S_T / S_C > N > 1$, we have to impose the following conditions: $(\delta_{ech,T})_C << 0.156 / S_T$ and $(\delta_{ech,C})_C << 0.156 / S_C$. Using the results of the scale analysis, the validity of the scale analysis is bounded by the condition:

$$RaN >> S_T / [m(1 - mS_C / S_T)] \quad (35)$$

- In all the other cases, the validity of the scale analysis requires: $(\delta_{ech,T})_T << 0.156 / S_T$ and $(\delta_{ech,C})T << 0.156 / S_C$. Eq. (36) is the result:

$$Ra >> S_C / [m(1 - mS_T / S_C)] \quad (36)$$

4. NUMERICAL MODELING

Defining $U = -\partial\Psi / \partial X$ and $V = \partial\Psi / \partial Y$, the dimensionless stream-function formulation of the governing equations is given by Eqs. (37)−(39):

$$\frac{\partial^2 \Psi}{\partial Y^2} + \frac{\partial^2 \Psi}{\partial X^2} = Ra \cdot \left(\frac{\partial \theta}{\partial Y} + N \frac{\partial \varphi}{\partial Y} \right) \quad (37)$$

$$\frac{\partial \theta}{\partial \tau} + \frac{\partial \Psi}{\partial Y}\frac{\partial \theta}{\partial X} + S_T \frac{\partial \Psi}{\partial Y} - \frac{\partial \Psi}{\partial X}\frac{\partial \theta}{\partial Y} = \frac{\partial^2 \theta}{\partial X^2} + \frac{\partial^2 \theta}{\partial Y^2} \quad (38)$$

$$\frac{\partial \varphi}{\partial \tau} + \frac{\partial \Psi}{\partial Y}\frac{\partial \varphi}{\partial X} + S_C \frac{\partial \Psi}{\partial Y} - \frac{\partial \Psi}{\partial X}\frac{\partial \varphi}{\partial Y} = \frac{1}{Le}\left(\frac{\partial^2 \varphi}{\partial X^2} + \frac{\partial^2 \varphi}{\partial Y^2} \right) \quad (39)$$

while the boundary conditions are:

$$\Psi = 0 \,;\, \theta = 1 - S_T \cdot X \,;\, \varphi = 1 - S_c \cdot X \text{ at } Y = 0$$
$$\frac{\partial \Psi}{\partial Y} = 0 \,,\; \theta = \varphi = 0 \text{ as } Y \to \infty \,.$$
$$\Psi = 0 \,,\; \theta = \varphi = 0 \text{ at } X = 0$$
$$\frac{\partial^2 \psi}{\partial X^2} = \frac{\partial^3 \psi}{\partial X^3} = \frac{\partial^2 \theta}{\partial X^2} = \frac{\partial^2 \varphi}{\partial X^2} = 0 \text{ at } X = H \quad (40)$$

The governing equations, Eqs. (37)−(39), subjected to the boundary conditions Eq. (40), were solved numerically using the finite difference method, the higher order hybrid scheme [14], [15]. The program was tested with good results (see Table 1) using the boundary conditions and the results already published in the literature [16, 17].

Table 1. Nusselt and Sherwood number compared with the results of the scientific literature [16, 17].

		Ra	400	100
Reference		Le		
Getachew e.a. [16]	Nu/Sh	1	7.58	3.07
This work	Nu/Sh		7.52	3.01
Getachew e.a. [16]	Nu	10	7.58	3.07
	Sh		27.90	13.10
Benacer e.a. [17]	Nu		7.77	3.11
	Sh		29.36	13.24
This work	Nu		7.75	3.02
	Sh		28.27	12.83

5. RESULTS AND DISCUSSIONS

An numerical example is presented for: $Ra = 600$, $B = 1.0$, $Le = 1$, $S_C = 0.07$ and $S_T = 0.05$. A computational domain of 0.4 x 30.0 was divided uniformly using 41 x 3001 points.

The iterative process required for solving the conservation equations was interrupted when a relative error of 10^{-6} of all the variables (temperature, concentration and stream function) is attained. Figure 4 presents the temperature (Fig. 4(a)), concentration (Fig. 4(b)),, vertical velocity (Fig. 4(c)), $(\partial\theta / \partial X) / S_T$ (Fig. 4(d)), $(\partial\varphi / \partial X) / S_C$ (Fig. 4(e)) contour plots as well as the $(1 - S_T) / N / (1 - S_C)$−X plot (Fig. 4(f)).

We notice negative values for the dimensionless temperature (Fig. 4(a)) and concentration (Fig. 4(b)) beyond $1 / S_T = 20.0$ and $1 / S_C = 14.28$ abscissas, respectively.

The point on the wall where the vertical velocity becomes null, the upper limit (UL), is given by the scale analysis as being $(1 + N) / (S_T + NS_C) = 16.67$, and this value is encountered in the finite difference analysis results (Fig. 4(c)). We notice, also, (Fig. 4(d)) that $(\partial\theta / \partial X) / S_T$ becomes smaller than 1.0 at the abscissa $X = 3$, while the scale analysis indicates a good approximation of $m / S_T = 3.11$.

Similarly, Fig. 4(e) shows a decrease of $(\partial\varphi / \partial X) / S_C$ bellow 1.0 for $X > 2$, while an abscissa of $m / S_C = 2.22$ is indicated successfully by the scale analysis. The fact that we have only a HDC regime, in this example, is shown clearly by Fig. 4(f) as $(1 - S_T) / N / (1 - S_C)$ has values greater than 1.0 in every point of the wall.

Three heat transfer regimes are encountered: $HDC_{T\text{-}C}$, in the $[0, m / S_C]$ region, followed by a $HDC_{T\text{-}Sc}$, regime in the $[m / S_C, m / S_T]$ region, and a $HDC_{St\text{-}Sc}$ regime in the $[m / S_T, UL]$ region.

Three abscissas were considered for each region and unscaled and scaled temperature,

concentration and vertical velocity graphs are presented by Figs. 5-7.

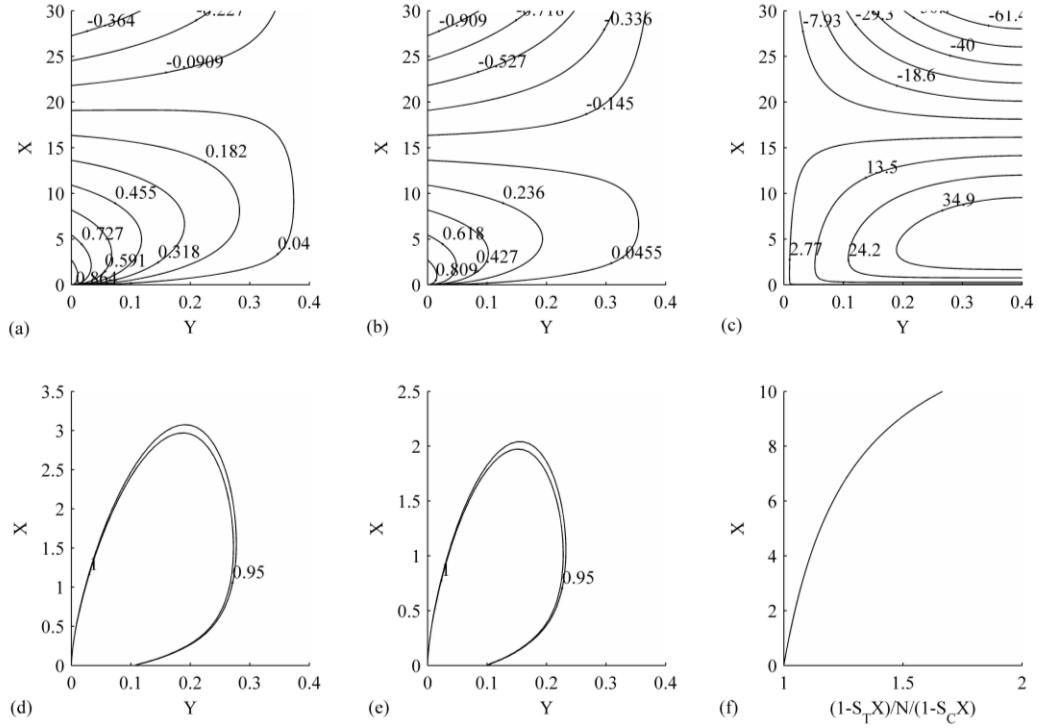

Fig. 4: The temperature (a), the concentration (b), the vorticity (c), $(\partial\theta/\partial X)/S_T$ (d), $(\partial\varphi/\partial X)/S_C$ (e) fields and the $(1-S_T)/N/(1-S_C)$−X plot (f) for $Ra=600$, $B=1.0$, $Le=1$, $S_C=0.07$ and $S_T=0.05$.

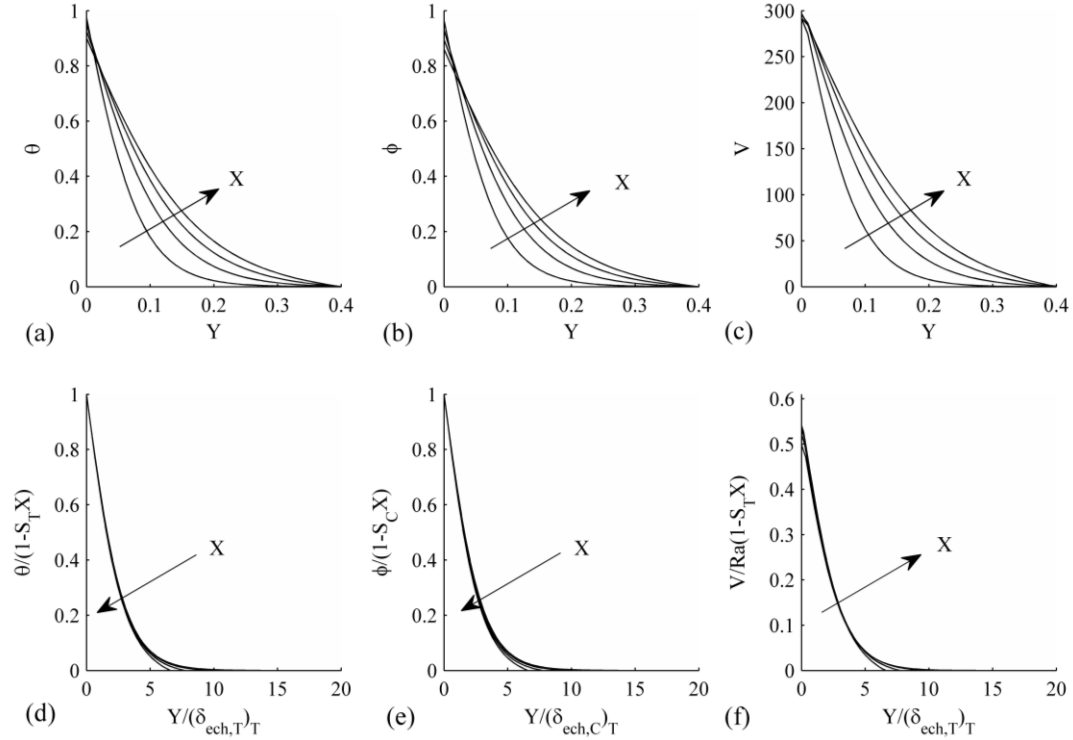

Fig. 5: The temperature, concentration and vertical velocity field variation as a function of Y co-ordinate (Fig. 5(a)−(c)), and the scaled temperature, concentration and vertical velocity field variation as a function of the scaled ordinate (Fig. 5(d)−(f)), for four $HDC_{C,T}$ abscissas: 0.5, 1.0, 1.5 and 2.0, $Ra=600$, $B=1.0$, $Le=1$, $S_C=0.07$ and $S_T=0.05$.

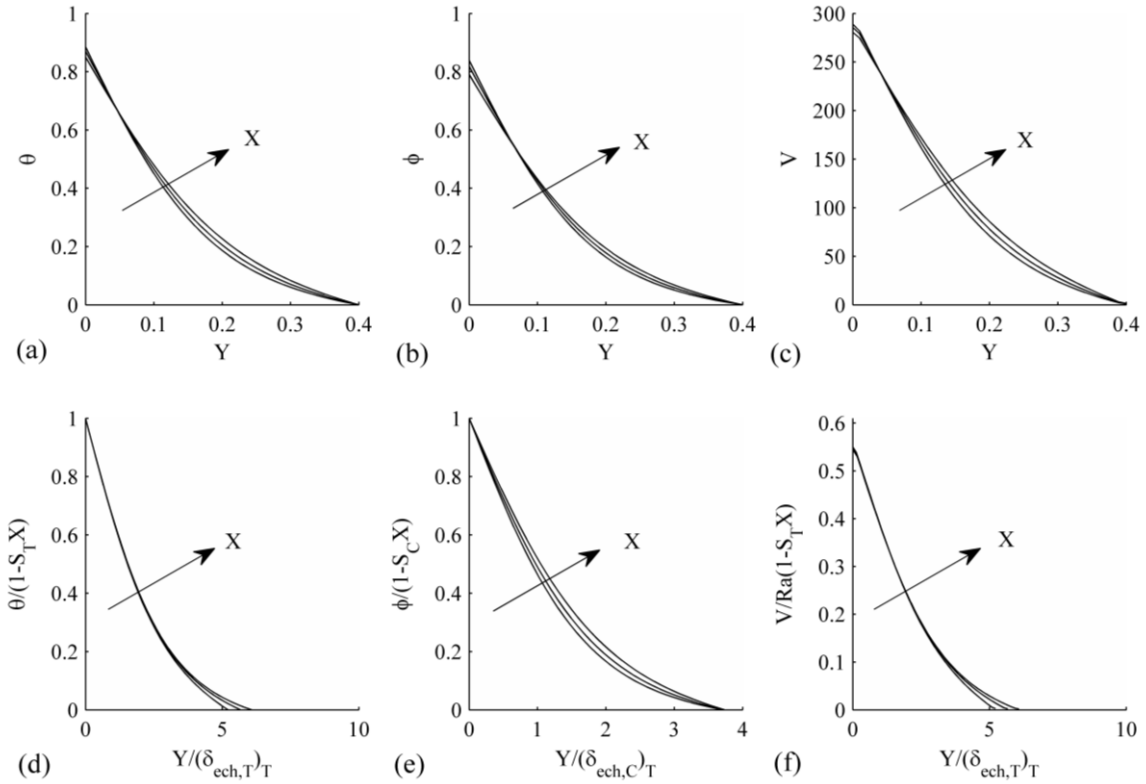

Fig. 6: The temperature, concentration and vertical velocity field variation as a function of Y co-ordinate (Fig. 6(a)−(c)), and the scaled temperature, concentration and vertical velocity field variation as a function of the scaled ordinate (Fig. 6(d)−(f)), for three $HDC_{Sc,T}$ abscissas: 2.3, 2.6 and 3.0, $Ra = 600$, $B = 1.0$, $Le = 1$, $S_C = 0.07$ and $S_T = 0.05$.

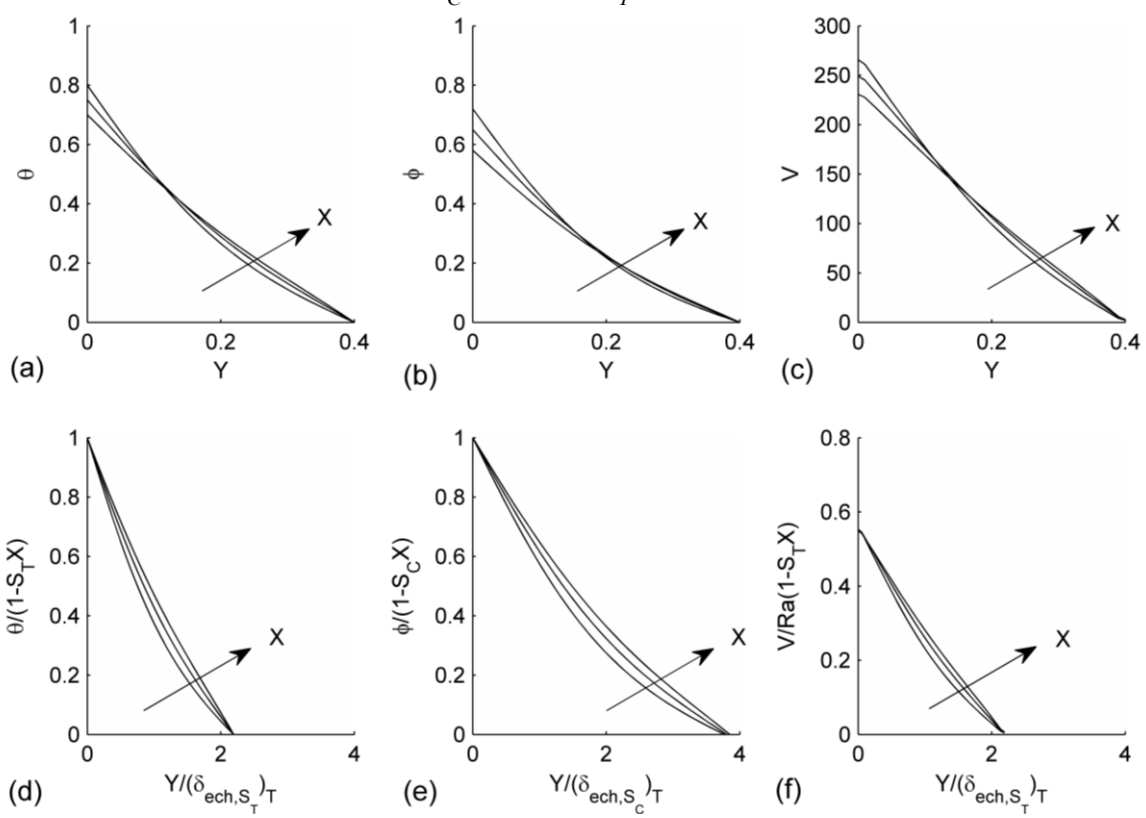

Fig. 7: The temperature, concentration and vertical velocity field variation as a function of Y co-ordinate (Fig. 7(a)−(c)), and the scaled temperature, concentration and vertical velocity field variation as a function of the scaled ordinate (Fig. 7(d)−(f)), for three $HDC_{Sc,St}$ abscissas: 4.0, 5.0 and 6.0, $Ra = 600$, $B = 1.0$, $Le = 1$, $S_C = 0.07$ and $S_T = 0.05$.

Figure 5. presents temperature (Fig. 5(a)), concentration (Fig. 5(b)), vertical velocity (Fig.5(c)) as well as their scaled versions (Figs. 5(d-f)) for four abscissas: 0.5, 1.0, 1.5, 2.0, in the $HDC_{T\text{-}C}$ region.

Figure 6 presents the temperature (Fig. 6(a)), concentration (Fig. 6(b)), vertical velocity (Fig. 6(c)) as well as their scaled versions (Figs. 6(d-f)) for the abscissas: 2.3, 2.6, 3.0, situated in the $HDC_{T\text{-}Sc}$ region.

Figure 7 presents temperature (Fig. 7(a)), concentration (Fig. 7(b)), vertical velocity (Fig. 7(c)) as well as their scaled versions (Figs. 7(d-f)) for three abscissas: 4.0, 5.0 and 6.0, situated in the $HDC_{St\text{-}Sc}$ region.

The collapse of all the scaled graphs shows the validity of the scale analysis for all the three regions encountered in this example.

6. CONCLUSIONS

This paper establishes heat and/or mass driven convection regimes that drive the steady state natural convection near a vertical impermeable wall of constant temperature and concentration embedded in a Darcy doubly stratified porous medium.

The scale analysis of the system shows the following situations that we can encounter:

- if $S_C > S_T$ only a HDC regime attains the equilibrium state;
- if $S_T / S_C > N > 1$ only a MDC regime can be registered, while
- in all the other cases a HDC − MDC regimes succession is encountered.

These results were verified with good results for one particular case using the finite difference method solutions of the governing equations.

The maps of the convection regimes give us a better understanding of the natural convection processes for the case analyzed in this paper.

REFERENCES

[1] **R. S. Telles, O. V. Trevisan**, *Dispersion in heat and mass transfer natural convection along vertical boundaries in porous media*, International Journal of Heat and Mass Transfer 36 (5), 1993, pag. 1357−1365.

[2] **D. Angirasa, G. P. Peterson**, *Natural convection heat transfer from an isothermal vertical surface to a fluid saturated thermally stratified porous medium*, International Journal of Heat and Mass Transfer 40 (18), 1997, pag. 4329−4335.

[3] **K. Tewari. P. Singh**, *Natural convection in a thermally stratified fluid saturated porous medium,* International Journal of Engineering Science 30 (8), 1992, pag. 1003−1007.

[4] **P. Singh, K. Tewari**, *Non-Darcy free convection from vertical surfaces in thermally stratified porous media*, International Journal of Engineering Science 31 (9), 1993, pag. 1233−1242.

[5] **I. Y. Hussain, B. K. Raheem**, *Natural convection heat transfer from a plane wall to thermally stratified porous media*, International Journal of Computer Applications 65 (1), 2013, pag. 42−49.

[6] **P. Singh, K. Sharma**, *Integral method to free convection in thermally stratified porous medium*, Acta Mechanica 83 (3−4), 1990, pag. 157−163.

[7] **I. Pop, H. Herwig**, *Transient mass transfer from an isothermal vertical flat plate embedded in a porous medium*, International Communications in Heat and Mass Transfer 17 (6), 1990, pag. 813−821.

[8] **J.-Y. Jang, J.-R. Ni**, *Transient free convection with mass transfer from an isothermal vertical flat plate embedded in a porous medium*, International Journal of Heat and Fluid Flow 10 (1), 1989, pag. 59−65.

[9] **A. Bejan, K. R. Khair**, *Heat and mass transfer by natural convection in a porous medium*, International Journal of Heat and Mass Transfer 28 (5), 1985, pag. 909−918.

[10] **D. Angirasa, G. P. Peterson, I. Pop**, *Combined heat and mass transfer by natural convection with opposing buoyancy effects in a fluid saturated porous medium*, International Journal of Heat and Mass Transfer 40 (12), 1997, pag. 2755−2773.

[11] **C. Allain, M. Cloitre, A. Mongruel**, *Scaling in flows driven by heat and mass convection in a porous medium*, Europhysics Letters 20 (4), 1992, pag. 313−318.

[12] **P. A. Lakshmi Narayana, P. V. S. N. Murthy**, *Free convective heat and mass transfer in a doubly stratified non-darcy porous medium*, ASME Journal of Heat Transfer 128 (11), 2006, pag. 1204−1212.

[13] **A. Bejan**, *Convection Heat Transfer*, second ed., Wiley, New York, 1995, pag. 18−21, pag. 535-539.

[14] **C. A. J. Fletcher**, *Computational Techniques for Fluid Dynamics 1. Fundamental and General Techniques*, second ed., Springer-Verlag New York, 1991, pag. 296-299.

[15] **J. C. Tannehill, D. A. Anderson, R. H. Pletcher**, *Computational Fluid Mechanics and Heat Transfer*, second ed., Taylor&Francis, Washington, 1997, pag. 45−70.

[16] **D. Getachew, D. Poulikakos, W. J. Minkowycz**, *Double diffusion in a porous cavity saturated with non-Newtonian fluid*, Journal of Thermophysics and Heat Transfer 12 (3), 1998, pag. 437−446.

[17] **R. Bennacer, A. Tobbal, H. Beji, P. Vasseur**, *Double diffusive convection in a vertical enclosure filled with anisotropic porous media*, International Journal of Thermal Sciences 40 (1), 2001, pag. 30-41.